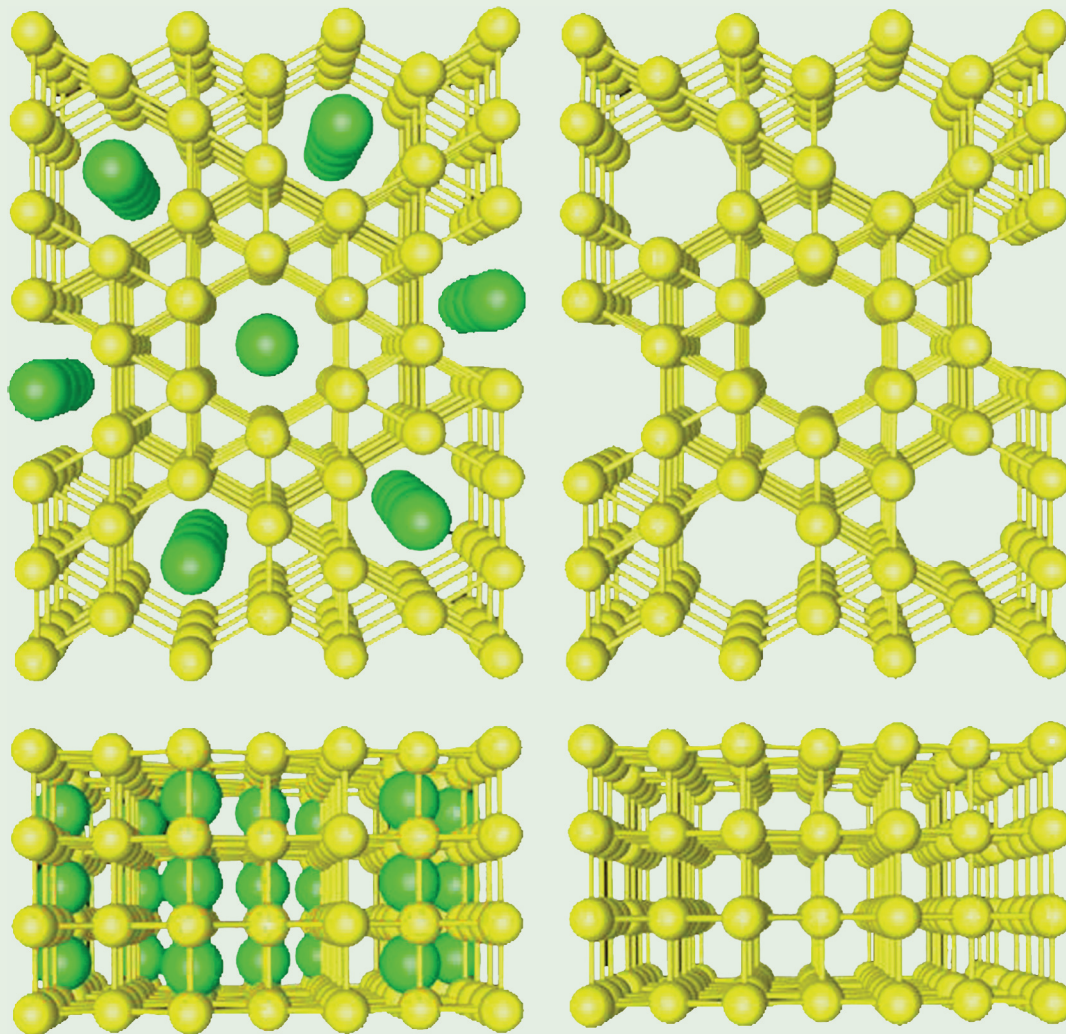


PHYSICAL REVIEW LETTERS

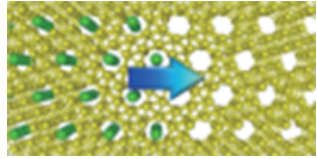
Articles published week ending

13 APRIL 2018



Dear Sir or Madam,

We are pleased to inform you that the Letter



Superconducting open-framework allotrope of silicon
at ambient pressure

Ha-Jun Sung, W.H. Han, In-Ho Lee, and K.J. Chang
Phys. Rev. Lett. **120**, 157001 (2018)

Published 11 April 2018

has been highlighted by the editors as an Editors' Suggestion. Publication of a Letter is already a considerable achievement, as *Physical Review Letters* accepts fewer than 1/4 of submissions, and is ranked first among physics and mathematics journals by the Google Scholar five-year h-index. A highlighted Letter has additional significance, because only about one Letter in six is highlighted as a Suggestion due to its particular importance, innovation, and broad appeal. Suggestions are downloaded twice as often as the average Letter, and are covered in the press substantially more often. If Suggestions were a separate publication, they would have an Impact Factor of 14. More information about our journal and its history can be found on our webpage prl.aps.org.

Yours sincerely,

Hugues Chaté
Editor
Physical Review Letters

Michael Thoennessen
Editor in Chief
Physical Review

Superconducting Open-Framework Allotrope of Silicon at Ambient Pressure

Ha-Jun Sung,¹ W. H. Han,¹ In-Ho Lee,² and K. J. Chang^{1,*}

¹Department of Physics, Korea Advanced Institute of Science and Technology, Daejeon 34141, Korea

²Korea Research Institute of Standards and Science, Daejeon 34113, Korea



(Received 16 August 2017; published 11 April 2018; corrected 13 April 2018)

Diamond Si is a semiconductor with an indirect band gap that is the basis of modern semiconductor technology. Although many metastable forms of Si were observed using diamond anvil cells for compression and chemical precursors for synthesis, no metallic phase at ambient conditions has been reported thus far. Here we report the prediction of pure metallic Si allotropes with open channels at ambient pressure, unlike a cubic diamond structure in covalent bonding networks. The metallic phase termed $P6/m\text{-Si}_6$ can be obtained by removing Na after pressure release from a novel Na-Si clathrate called $P6/m\text{-NaSi}_6$, which is predicted through first-principles study at high pressure. We identify that both $P6/m\text{-NaSi}_6$ and $P6/m\text{-Si}_6$ are stable and superconducting with the critical temperatures of about 13 and 12 K at ambient pressure, respectively. The prediction of new Na-Si and Si clathrate structures presents the possibility of exploring new exotic allotropes useful for Si-based devices.

DOI: 10.1103/PhysRevLett.120.157001

Silicon is an abundant, nontoxic element in the Earth's crust and widely used as the key material for electronic devices, such as integrated circuits and solar cells. At ambient conditions, Si crystallizes in a cubic diamond structure and also exists in numerous metastable forms, such as amorphous Si, porous Si, Si nanostructures (nanowires and silicene), and Si clathrates. It is known that Si forms various metallic phases under compression, following the transition sequence from cubic diamond (CD-Si, Si-I) to β -Sn (Si-II) to *Imma*-Si (Si-XI) to simple hexagonal (SH-Si, Si-V) to *Cmca*-Si (Si-VI) to hexagonal close-packed (Si-VII) to face-centered cubic (Si-X) [1–4]. Upon slow pressure release from the β -Sn phase, Si does not recover the cubic diamond phase, but instead transforms to other metastable phases with distorted tetrahedral bonds, such as rhombohedral R8 (Si-XII) and body-centered BC8 (Si-III) phases [5,6]. Subsequent thermal annealing of BC8-Si leads to the formation of hexagonal diamond Si (Si-IV) [5,6]. Upon fast release of pressure, two metastable phases referred to as Si-VIII and Si-IX were obtained, but their crystal structures have not been identified yet [7]. Besides that, an unidentified Si-XIII phase was discovered upon thermal annealing of the R8/BC8 mixture made by indentation [8]. Recently, based on the combined study of *ab initio* calculations and microexplosion experiments, two new structures called BT8 and ST12 were identified on Si surface exposed to ultrashort laser pulses [9].

Another route for synthesizing other Si allotropes is to use appropriate chemical precursors followed by physical and chemical manipulations. In this process, thermodynamically stable precursors can be produced under pressure and may maintain their stability to ambient conditions. In Na-Si systems, the type-II Si clathrate ($Fd\bar{3}m\text{-Si}_{136}$) with

cages has been synthesized by removing Na from the precursor of type-II $Na_{24}\text{Si}_{136}$ clathrate [10,11], while Na has not been successfully removed from the cages of type-I $Na_8\text{Si}_{46}$ clathrate. Recently, a new $Na_4\text{Si}_{24}$ clathrate was made at high pressure, and its crystal structure was maintained at ambient pressure [12]. Through a thermal degassing process, a new Si_{24} clathrate with open channels, hereafter referred to as *Cmcm*-Si₆, was obtained from the $Na_4\text{Si}_{24}$ precursor, possessing a quasidirect band gap near 1.3 eV [13]. Although the reported metastable Si allotropes (Si-IV, BC8, R8, ST12, BT8, $Fd\bar{3}m\text{-Si}_{136}$, and *Cmcm*-Si₆) can persist to ambient conditions, all of them are semiconducting [5,6,9–11,13], and metallic Si phases at ambient conditions have not been reported to date. Theoretically, BC8-Si was predicted to be a semimetal [14–16], but it has been recently confirmed as a narrow gap semiconductor from optical, electrical, and heat capacity measurements on phase-pure bulk samples [17]. The superconductivity of Si has been observed in heavily *B*-doped cubic diamond phase [18] and β -Sn and simple hexagonal phases under pressure [19–21]. However, the high-pressure metallic phases do not maintain their crystal structures after the release of pressure [5–7].

Here we report the prediction of a new Na-Si clathrate structure, which can be synthesized at high pressure and used as a precursor to obtain a novel superconducting Si phase at ambient pressure. The new clathrate structure, termed $P6/m\text{-NaSi}_6$, contains open channels embedded in a simple hexagonal Si lattice and guest Na atoms filling the channels. The enthalpy of $P6/m\text{-NaSi}_6$ is lower than that of the recently discovered $Na_4\text{Si}_{24}$ clathrate above 12.4 GPa, and its stability is verified by phonon spectra and molecular dynamics simulations. We find that a novel metallic phase

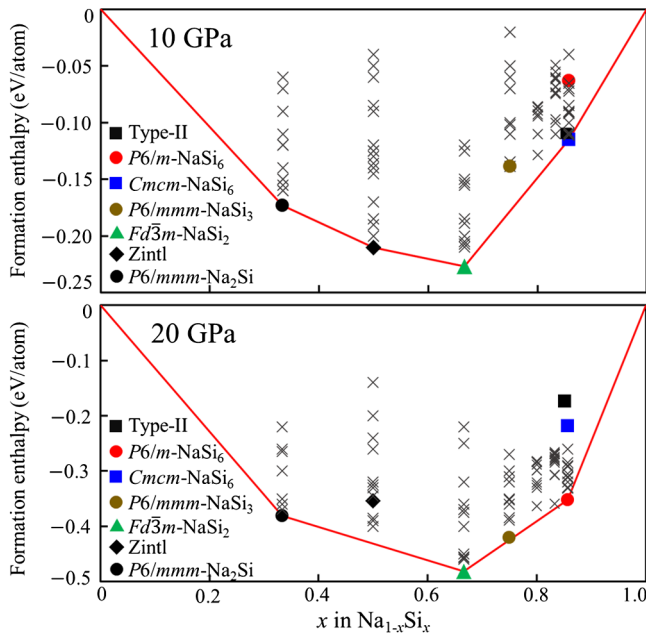


FIG. 1. Formation enthalpies of stable and metastable configurations for $\text{Na}_{1-x}\text{Si}_x$ with various composition ratios at pressures of 10 GPa (top) and 20 GPa (bottom). The configurations on the convex hull are marked by solid symbols and connected by red lines.

termed $P6/m\text{-Si}_6$ can be obtained through the thermal degassing from $P6/m\text{-NaSi}_6$, and both $P6/m\text{-NaSi}_6$ and $P6/m\text{-Si}_6$ exhibit the superconducting behavior at ambient pressure.

We explored new Na-Si clathrates at high pressure using an *ab initio* evolutionary crystal structure search method [22]. The enthalpy minimization and electronic structure calculations were performed within the framework of density-functional theory (full details can be found in the Supplemental Material [23]). We considered Na-Si systems with various composition ratios, Na_xSi_y ($x: y = 2: 1, 1: 1, 1: 2, 1: 3, 1: 4, 1: 5, 1: 6$), each of which contains up to three formula units per supercell. The formation enthalpies of Na_xSi_y are plotted for the stable and metastable configurations at 10 and 20 GPa (Fig. 1). The configurations on the convex hull are enthalpically stable against the decomposition into Na metal and CD-Si. At 10 GPa, NaSi with $x: y = 1: 1$ crystallizes in a Na_4Si_4 Zintl phase lying on the convex hull. For $x: y = 1: 6$, our crystal structure search method reproduces the clathrate structure of $\text{Na}_4\text{Si}_{24}$ in the orthorhombic $Cmcm$ space group (hereafter referred to as $Cmcm\text{-NaSi}_6$), which has been recently discovered via high-pressure synthesis [12]. For Na_2Si and NaSi_2 systems, we find the stable structures in the $P6/mmm$ and $Fd\bar{3}m$ space groups (see Supplemental Material [23], Fig. 1), respectively, both of which have been theoretically proposed for Li-Si, Ba-Si, and Ca-Si compounds [32–34].

As pressure increases to 20 GPa, the Zintl phase becomes unstable against decomposition and NaSi_3 forms

a hexagonal layered structure in the $P6/mmm$ space group, which consists of alternating hexagonal and triangular Si rings (see Supplemental Material [23], Fig. 1), similar to the low-pressure phase predicted for LiSi_3 [34]. For NaSi_6 systems, we find a very distinctive clathrate structure in the hexagonal $P6/m$ space group [Fig. 2(a)]. The new NaSi_6 clathrate, termed $P6/m\text{-NaSi}_6$, maintains its crystal structure and symmetry even after pressure is released. At ambient pressure, $P6/m\text{-NaSi}_6$ has the equilibrium lattice parameters $a = b = 7.038$ and $c = 2.573$ Å and two inequivalent Wyckoff positions, $1a$ (0, 0, 0.5) and $6j$ (0.145, 0.710, 0), for the Na and Si atoms, respectively. The $P6/m\text{-NaSi}_6$ clathrate consists of sevenfold Si atoms and contains open channels along the crystallographic c axis. The open channels are formed from six-membered Si rings. The intercalated Na atoms along the open channels are sandwiched between hexagonal Si layers. If the Si atoms are added to fill the open channels after removing the Na atoms, the crystal structure is exactly the same as a simple hexagonal lattice, which is known as the stable metallic phase of Si at pressures of 13.2–39.2 GPa [1,2]. Although various clathrate forms have been studied for Li-, Ca-, and Ba-Si systems at high pressure [32–34], to our knowledge, the $P6/m$ structure of NaSi_6 has not been reported yet.

For the composition ratio of $x: y = 1: 6$, the stability of $P6/m\text{-NaSi}_6$ was compared with the known Na-Si clathrates under pressure by calculating the enthalpy difference per atom defined with respect to a mixture of Zintl and CD-Si,

$$\Delta H = [H(\text{Na}_x\text{Si}_y) - xH(\text{NaSi}) - (y-x)H(\text{CD-Si})]/(x+y), \quad (1)$$

where $H(\text{Na}_x\text{Si}_y)$, $H(\text{NaSi})$, and $H(\text{CD-Si})$ are the enthalpies of Na_xSi_y clathrate, Zintl, and CD-Si, respectively. For the type-I ($\text{Na}_8\text{Si}_{46}$) and type-II ($\text{Na}_{24}\text{Si}_{136}$) clathrates with different stoichiometries from NaSi_6 , we chose the $(\text{NaSi}_{5.75} + 0.25 \text{ CD-Si})$ and $(\text{NaSi}_{5.667} + 0.333 \text{ CD-Si})$ systems, respectively. The relative enthalpies are plotted as a function of pressure in Fig. 2(b). The $Cmcm\text{-NaSi}_6$ clathrate is enthalpically more favorable than the type-I clathrate at 7.7 GPa, in good agreement with the previous study [12]. As pressure increases above 12.4 GPa, the $P6/m\text{-NaSi}_6$ clathrate becomes the most stable phase.

The thermal stability of $P6/m\text{-NaSi}_6$ was examined by carrying out first-principles isothermal-isobaric molecular dynamics (NpT -MD) simulations at 15 GPa and 1000 K. For a $2 \times 2 \times 6$ supercell containing 144 Si atoms and 24 Na atoms, $P6/m\text{-NaSi}_6$ was found to be stable up to 100 ps (see Supplemental Material [23], Fig. 2). Furthermore, we calculated the full phonon spectra and found no imaginary phonon modes, identifying the dynamical stability of $P6/m\text{-NaSi}_6$ [Fig. 3(a)]. Based on the enthalpy vs pressure curves and NpT -MD simulations, we suggest that the synthesis of $P6/m\text{-NaSi}_6$ is possible under high-temperature conditions

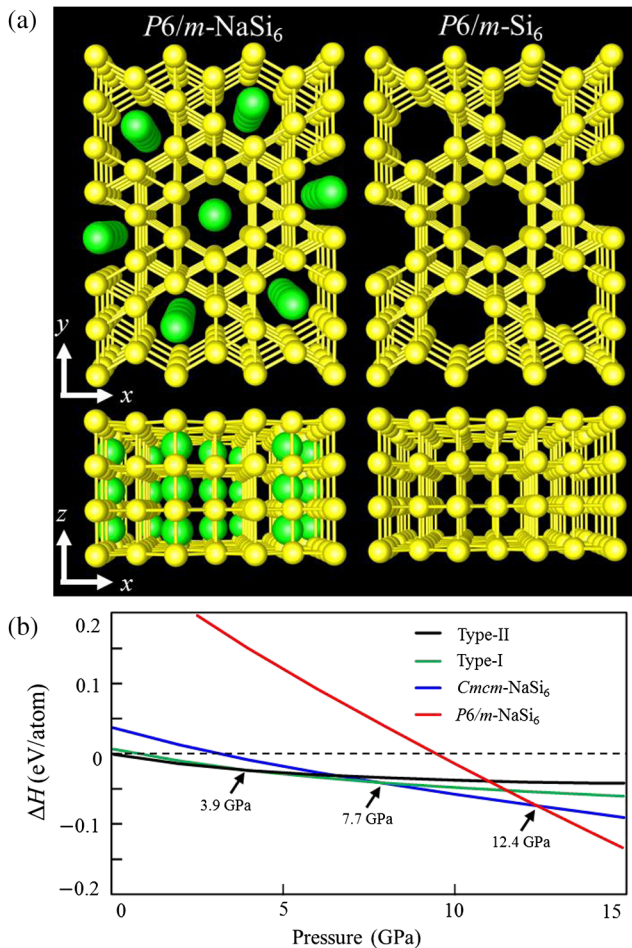


FIG. 2. (a) Top and side views of the atomic structures of $P6/m$ -NaSi₆ (left) and $P6/m$ -Si₆ (right) clathrates. In $P6/m$ -NaSi₆, the open channels filled with Na atoms are embedded in the metallic bonding networks of Si atoms that are exactly the same as that of a simple hexagonal lattice except for the open channels. The green and yellow spheres represent Na and Si atoms, respectively. (b) Relative enthalpies (ΔH) of various clathrate structures with respect to a mixture of Zintl and CD-Si as a function of pressure.

above 12.4 GPa. In addition, to guide the experimental identification of $P6/m$ -NaSi₆, we simulated the x-ray diffraction pattern at 12.4 GPa (see Supplemental Material [23], Fig. 3). To examine the stability of $P6/m$ -NaSi₆ at ambient pressure, we performed NpT -MD simulations at 400 K and found $P6/m$ -NaSi₆ to be stable up to 100 ps (see Supplemental Material [23], Fig. 2). In addition, the dynamical stability of $P6/m$ -NaSi₆ at ambient pressure was convinced by phonon spectra calculations (see Supplemental Material [23], Fig. 4). We also confirmed that the elastic constants meet the criteria for mechanical stability in hexagonal structures [35].

When pressure is released from the $P6/m$ phase of NaSi₆, one can remove the Na atoms from the open channels using a thermal degassing process and subsequently obtain a new Si allotrope in the space group

$P6/m$, identical to the SH phase, except having open channels along the c axis [Fig. 2(a)]. Experiments have shown that the Na atoms can be removed by exposing Na-Si clathrates to elevated temperatures [10,11,13]. This degassing process occurs at temperatures of 623–648 K for the type-II clathrate with polyhedral cavities [10]. In $Cmcm$ -NaSi₆, the Na removal leading to the $Cmcm$ -Si₆ allotrope was achieved at a lower temperature of 400 K due to the presence of open channels [13]. Since $P6/m$ -NaSi₆ has open channels, the degassing process can also remove the Na atoms at relatively low temperatures. Using a climbing image nudged elastic band method [31], we investigated the migration of Na along the open channels for both the $Cmcm$ - and $P6/m$ -NaSi₆ allotropes and estimated the energy barriers for Na migration to be 0.65 and 0.48 eV at zero pressure, respectively (see Supplemental Material [23], Fig. 5). The lower energy barrier of $P6/m$ -NaSi₆ is because the large open channels are connected in a straight line to weaken the interaction between the guest and its surrounding Si atoms. We performed MD simulations to examine the stability of Si-based lattice in $P6/m$ -NaSi₆ during the degassing process at 400 K and found that the Na diffusion does not affect the stability of the Si-based hexagonal lattice (see Supplemental Material [23], Fig. 6). Our results suggest that the $P6/m$ -Si₆ allotrope can be formed at temperatures around 400 K through the degassing process, similar to $Cmcm$ -Si₆. The lattice parameters of $P6/m$ -Si₆ after the Na removal are reduced to $a = b = 6.854$ and $c = 2.478$ Å. Since the $P6/m$ -Si₆ structure is composed of highly coordinated Si atoms, this high-density phase is metallic, unlike the low-density $Cmcm$ -Si₆ allotrope having a semiconducting band gap due to fourfold coordinated Si atoms.

The electronic band structures of $P6/m$ -NaSi₆ and $P6/m$ -Si₆ are compared in Fig. 3(b). In the type-I, type-II, and $Cmcm$ -NaSi₆ clathrates, all Si atoms are tetrahedrally bonded within an sp^3 covalent network, as in the diamond phase. Thus, these clathrates exhibit the semiconducting band structure after the guest atoms are removed [10,11,13]. In $P6/m$ -NaSi₆, although the Na degassing process lowers the Fermi level, the metallic band structure persists for $P6/m$ -Si₆. The SH phase of Si was observed to be superconducting with a critical temperature of 8.2 K at 15.2 GPa [20,21]. Similar to SH-Si, both $P6/m$ -NaSi₆ and $P6/m$ -Si₆ have the metallic bonding network and high electronic density of states as ingredients for superconductivity.

To explore the superconductivity of $P6/m$ -NaSi₆ and $P6/m$ -Si₆, the electron-phonon (EP) coupling constant λ was calculated from density-functional perturbation theory (full details in Supplemental Material [23]). The Allen-Dynes modified McMillan equation was used to estimate the superconducting critical temperature T_c [36,37], with choosing the Coulomb pseudopotential of $\mu^* = 0.1$. The

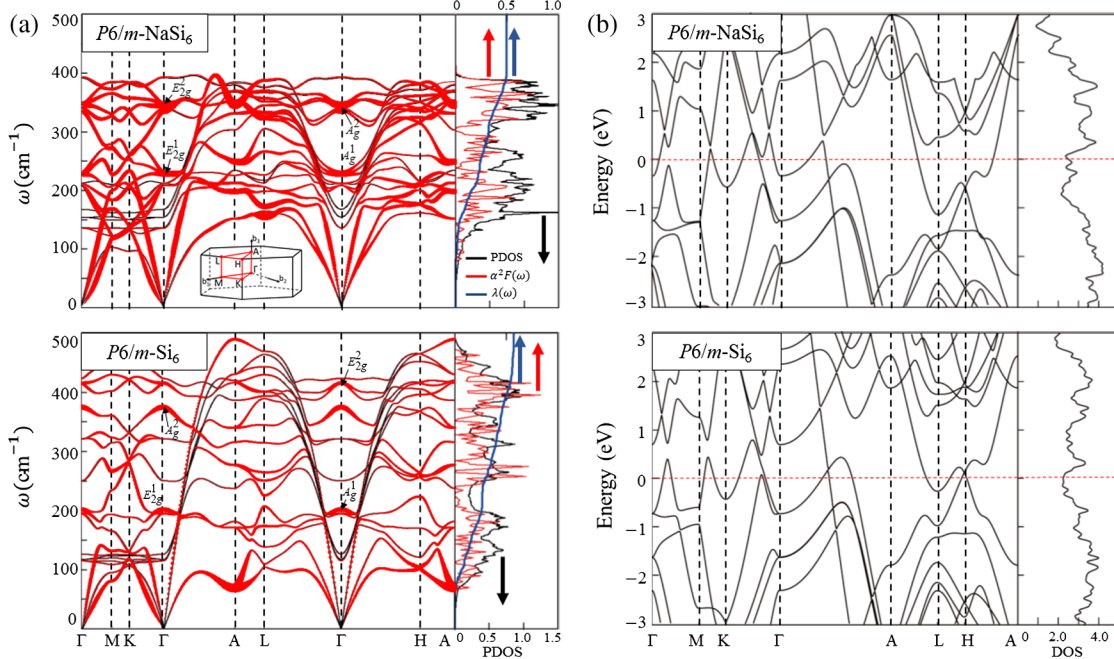


FIG. 3. (a) Phonon spectra, phonon densities of states (PDOS in arb. unit), Eliashberg spectral functions $\alpha^2 F(\omega)$, and electron-phonon couplings $\lambda(\omega)$ for *P*6/*m*-NaSi₆ (top) and *P*6/*m*-Si₆ (bottom) at 15 GPa. The magnitude of $\lambda(\omega)$ is indicated by the thickness of the red curves. (b) Band structures and electronic densities of states (DOS in arb. unit) of *P*6/*m*-NaSi₆ (top) and *P*6/*m*-Si₆ (bottom) at 15 GPa, with the Fermi level set to zero.

logarithmic average of phonon frequencies ω_{log} and frequency-dependent EP coupling $\lambda(\omega)$ were obtained from the Eliashberg spectral function $\alpha^2 F(\omega)$ [Fig. 3(a)]. The results for λ , ω_{log} , and T_c are compared for SH-Si, *P*6/*m*-NaSi₆, and *P*6/*m*-Si₆ (see Supplemental Material [23], Table I). The superconducting temperature of SH-Si is estimated to be 7.9 K at 15 GPa, in good agreement with the reported value [20,21]. We find that both the *P*6/*m*-NaSi₆ and *P*6/*m*-Si₆ allotropes are superconducting with the critical temperatures of 13.1 and 12.2 K at zero pressure, respectively. These T_c values are higher than those (4–8 K) observed for the high-pressure β -Sn and SH phases of Si [19–21] and the type-I clathrate of (Na, Ba)_xSi₄₆ and Ba₈Si₄₆ [38,39]. As pressure increases to 15 GPa, the critical temperature decreases to 4.0 K for *P*6/*m*-NaSi₆ and 5.3 K for *P*6/*m*-Si₆ [Fig. 4(a)]. The pressure coefficients of T_c are -0.61 and -0.46 K/GPa for *P*6/*m*-NaSi₆ and *P*6/*m*-Si₆, respectively, similar to the measured value of -0.52 K/GPa for SH-Si [20].

In both *P*6/*m*-NaSi₆ and *P*6/*m*-Si₆, there are four notable Raman active modes at the Γ point [Fig. 3(a)], A_g^1 and A_g^2 modes associated with torsional and breathing motions of Si atoms around the open channels, respectively, and E_{2g}^1 and E_{2g}^2 modes related to stretching and bending distortions of in-plane Si–Si bonds (see Supplemental Material [23], Fig. 7). In *P*6/*m*-NaSi₆, the interaction of the E_{2g}^1 optical modes with electrons is strong along Γ –A, A–L, and A–H in the Brillouin zone [Fig. 3(a)]. However, there are no specific phonon modes with

dominant contributions to the EP coupling. The density of states at the Fermi level $N(0)$ is higher in *P*6/*m*-NaSi₆ than *P*6/*m*-Si₆ (see Supplemental Material [23], Table I), and therefore the higher T_c of *P*6/*m*-NaSi₆ than *P*6/*m*-Si₆ at zero pressure is mainly related to $N(0)$. Since the EP coupling is weakened and $N(0)$ decreases under pressure (see Supplemental Material [23], Fig. 8), both *P*6/*m*-NaSi₆ and *P*6/*m*-Si₆ show the decreasing pressure behavior of T_c . In *P*6/*m*-Si₆, the transverse acoustic (TA) modes around the A point are softened under pressure, unlike

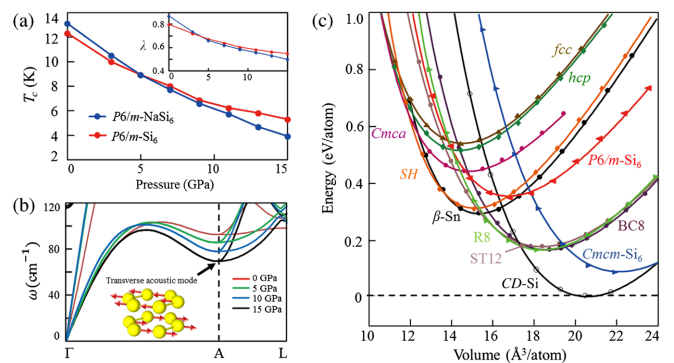


FIG. 4. (a) Pressure dependences of T_c and λ for *P*6/*m*-NaSi₆ and *P*6/*m*-Si₆. (b) Pressure variation of the low-frequency modes of *P*6/*m*-Si₆ along the Γ -A-L line in the BZ. The balls represent the Si atoms around the open channels and the arrows stand for the displacements of the TA mode at the A point. (c) Energy vs volume curves of various Si phases.

$P6/m$ -NaSi₆ [Fig. 4(b)]. Since the crystal volume is reduced after the Na removal, the phonon modes are more rigid in $P6/m$ -Si₆ than $P6/m$ -NaSi₆ [Fig. 3(a)]. Although ω_{log} is higher in $P6/m$ -Si₆ at zero pressure, its value becomes lower than that of $P6/m$ -NaSi₆ as pressure increases above 7 GPa (see Supplemental Material [23], Fig. 8). Because of the soft TA modes, the EP coupling of $P6/m$ -Si₆ appears strongly along $\Gamma - A$, $A - L$, and $A - H$ and is strengthened as pressure increases [Fig. 3(a)], resulting in a smaller pressure coefficient of T_c .

Finally, we discuss the stability of $P6/m$ -Si₆ at ambient pressure. The total energy of $P6/m$ -Si₆ is calculated to be about 0.35 eV/atom higher than that of CD-Si [Fig. 4(c)]. Since $P6/m$ -Si₆ is less stable by 0.26 eV/atom than $Cmcm$ -Si₆, its thermal stability is more sensitive to temperature. Nonetheless, we identified the thermal, dynamical, and mechanical stability of $P6/m$ -Si₆ up to 400 K at ambient pressure through NpT -MD simulations and calculations of the phonon spectra (see Supplemental Material [23], Figs. 2 and 4) and elastic constants [35]. When heated above 400 K, $P6/m$ -Si₆ forms an amorphouslike disordered structure and then may decompose or turn to the most stable CD-Si phase. In the type-II Na₂₄Si₁₃₆ clathrate, it is known that the guest atoms frustrate a transition into another phase at high pressure [40]. Similarly, in $P6/m$ -NaSi₆, the guest atoms residing along the open channels suppress the motions of the Si layers and thus maintain the structural stability even at high pressure. In $P6/m$ -Si₆, the TA modes at the A point are associated with the displacements of the hexagonal Si layers along the [110] and [1̄10] directions [Fig. 4(b)]. Since two adjacent layers move in opposite directions, the open channels can be broken by large atomic displacements. Although the instability of the TA modes leads to a transition to the hexagonal close-packed (hcp) structure under pressure, the energy vs volume curves show that $P6/m$ -Si₆ is likely to transform to a metallic $Cmca$ -Si phase (at 6.6 GPa) prior to the transition to hcp (at 12.1 GPa) [Fig. 4(c)].

In conclusion, we have predicted a new $P6/m$ -NaSi₆ clathrate that can be synthesized at high pressures above 12.4 GPa. The stability of $P6/m$ -NaSi₆ down to zero pressure has been verified through molecular dynamics simulations and calculations of the phonon spectra and elastic constants, although phase separation and long-term instability problems were not taken into account due to the limited supercell size and limited simulation time. Using the $P6/m$ -NaSi₆ clathrate as a precursor after pressure release, we expect that the Na degassing process can produce a pure metallic Si phase at ambient pressure, termed $P6/m$ -Si₆. Both the $P6/m$ -NaSi₆ and $P6/m$ -Si₆ allotropes are predicted to be superconducting with the critical temperatures of 13.1 and 12.2 K at zero pressure, respectively. The prediction of the novel superconducting Si phase not only provides a new paradigm for understanding the energy landscape of Si but offers an

opportunity to explore further exotic Si allotropes to be realized for new Si-based devices.

This work was supported by Samsung Science and Technology Foundation under Grant No. SSTF-BA1401-08.

*Corresponding author.

kjchang@kaist.ac.kr

- [1] J. Z. Hu and I. L. Spain, *Solid State Commun.* **51**, 263 (1984).
- [2] S. J. Duclos, Y. K. Vohra, and A. L. Ruoff, *Phys. Rev. B* **41**, 12021 (1990).
- [3] M. I. McMahon, R. J. Nelmes, N. G. Wright, and D. R. Allan, *Phys. Rev. B* **50**, 739 (1994).
- [4] M. Hanfland, U. Schwarz, K. Syassen, and K. Takemura, *Phys. Rev. Lett.* **82**, 1197 (1999).
- [5] R. H. Wentorf, Jr. and J. S. Kasper, *Science* **139**, 338 (1963).
- [6] J. Crain, G. J. Ackland, J. R. Maclean, R. O. Piltz, P. D. Hatton, and G. S. Pawley, *Phys. Rev. B* **50**, 13043(R) (1994).
- [7] Y.-X. Zhao, F. Buehler, J. R. Sites, and I. L. Spain, *Solid State Commun.* **59**, 679 (1986).
- [8] K. Mylvaganam, L. C. Zhang, P. Eyben, J. Mody, and W. Vandervorst, *Nanotechnology* **20**, 305705 (2009).
- [9] L. Rapp, B. Habel, C. J. Pickard, J. E. Bradby, E. G. Gamaly, J. S. Williams, and A. V. Rode, *Nat. Commun.* **6**, 7555 (2015).
- [10] J. Gryko, P. F. McMillan, R. F. Marzke, G. K. Ramachandran, D. Patton, S. K. Deb, and O. F. Sankey, *Phys. Rev. B* **62**, R7707 (2000).
- [11] S. Stefanoski, C. D. Malliakas, M. G. Kanatzidis, and G. S. Nolas, *Inorg. Chem.* **51**, 8686 (2012).
- [12] O. O. Kurakevych, T. A. Strobel, D. Y. Kim, T. Muramatsu, and V. V. Struzhkin, *Cryst. Growth Des.* **13**, 303 (2013).
- [13] D. Y. Kim, S. Stefanoski, O. O. Kurakevych, and T. A. Strobel, *Nat. Mater.* **14**, 169 (2015).
- [14] R. Biswas, R. M. Martin, R. J. Needs, and O. H. Nielsen, *Phys. Rev. B* **35**, 9559 (1987).
- [15] B. G. Pfrommer, M. Côté, S. G. Louie, and M. L. Cohen, *Phys. Rev. B* **56**, 6662 (1997).
- [16] B. D. Malone, J. D. Sau, and M. L. Cohen, *Phys. Rev. B* **78**, 035210 (2008).
- [17] H. Zhang, H. Liu, K. Wei, O. O. Kurakevych, Y. Le Godec, Z. Liu, J. Martin, M. Guerrette, G. S. Nolas, and T. A. Strobel, *Phys. Rev. Lett.* **118**, 146601 (2017).
- [18] E. Bustarret, C. Marcenat, P. Achatz, J. Kačmarčík, F. Lévy, A. Huxley, L. Ortéga, E. Bourgeois, X. Blase, D. Débarre, and J. Boullier, *Nature (London)* **444**, 465 (2006).
- [19] W. Buckel and J. Wittig, *Phys. Lett.* **17**, 187 (1965).
- [20] K. J. Chang, M. M. Dacorogna, M. L. Cohen, J. M. Mignot, G. Chouteau, and G. Martinez, *Phys. Rev. Lett.* **54**, 2375 (1985).
- [21] G. Martinez, J. M. Mignot, G. Chouteau, K. J. Chang, M. M. Dacorogna, and M. L. Cohen, *Phys. Scr. T13*, 226 (1986).
- [22] I.-H. Lee, Y. J. Oh, S. Kim, J. Lee, and K. J. Chang, *Comput. Phys. Commun.* **203**, 110 (2016).
- [23] See Supplemental Material at <http://link.aps.org/supplemental/10.1103/PhysRevLett.120.157001> for the details of calculation methods and the results for crystal

- volumes, $N(0)$, λ , ω_{log} , and T_c , x-ray diffraction pattern simulations, energy barriers for Na migration, and stability identification, which includes Refs. [22,24–31].
- [24] J. Lee, I.-H. Lee, and J. Lee, *Phys. Rev. Lett.* **91**, 080201 (2003).
 - [25] J. P. Perdew, K. Burke, and M. Ernzerhof, *Phys. Rev. Lett.* **77**, 3865 (1996).
 - [26] P. E. Blöchl, *Phys. Rev. B* **50**, 17953 (1994).
 - [27] G. Kresse and J. Furthmüller, *Phys. Rev. B* **54**, 11169 (1996).
 - [28] P. Giannozzi *et al.*, *J. Phys. Condens. Matter* **21**, 395502 (2009).
 - [29] D. Vanderbilt, *Phys. Rev. B* **41**, 7892(R) (1990).
 - [30] F. Izumi and K. Momma, *Solid State Phenom.* **130**, 15 (2007).
 - [31] G. Henkelman, B. P. Uberuaga, and H. Jónsson, *J. Chem. Phys.* **113**, 9901 (2000).
 - [32] G. Gao, N. W. Ashcroft, M. Miao, and R. Hoffmann, *J. Phys. Chem. C* **118**, 25167 (2014).
 - [33] J. Shi, W. Cui, J. A. Flores-Livas, A. San-Miguel, S. Botti, and M. A. L. Marques, *Phys. Chem. Chem. Phys.* **18**, 8108 (2016).
 - [34] S. Zhang, Y. Wang, G. Yang, and Y. Ma, *ACS Appl. Mater. Interfaces* **8**, 16761 (2016).
 - [35] Z.-J. Wu, E.-J. Zhao, H.-P. Xiang, X.-F. Hao, X.-J. Liu, and J. Meng, *Phys. Rev. B* **76**, 054115 (2007). For $P6/m\text{-NaSi}_6$ ($P6/m\text{-Si}_6$), the elastic constants at zero pressure were calculated to be 1143 (1229), 1934 (2810), 363 (210), 485 (795), and 391 (244) GPa for C_{11} , C_{33} , C_{44} , C_{12} , and C_{13} , respectively, satisfying the criteria for mechanical stability in hexagonal structures, $C_{44} > 0$, $C_{11} > |C_{12}|$, and $(C_{11} + 2C_{12})C_{33} > 2C_{13}^2$.
 - [36] W. L. McMillan, *Phys. Rev.* **167**, 331 (1968).
 - [37] P. B. Allen and R. C. Dynes, *Phys. Rev. B* **12**, 905 (1975).
 - [38] H. Kawaji, H.-O. Horie, S. Yamanaka, and M. Ishikawa, *Phys. Rev. Lett.* **74**, 1427 (1995).
 - [39] D. Connétable, V. Timoshevskii, B. Masenelli, J. Beille, J. Marcus, B. Barbara, A. M. Saitta, G.-M. Rignanese, P. Mélinon, S. Yamanaka, and X. Blase, *Phys. Rev. Lett.* **91**, 247001 (2003).
 - [40] A. San-Miguel, P. Kéghélian, X. Blase, P. Mélinon, A. Perez, J. P. Itié, A. Polian, E. Reny, C. Cros, and M. Pouchard, *Phys. Rev. Lett.* **83**, 5290 (1999).

Correction: The third sentence in the caption to Fig. 2 was inconsistent with the image and has been replaced. The author list in Ref. [30] contained an error and was corrected.

Supplemental Material

Superconducting open-framework allotrope of silicon at ambient pressure

Ha-Jun Sung,¹ W. H. Han,¹ In-Ho Lee,² and K. J. Chang^{1*}

¹*Department of Physics, Korea Advanced Institute of Science and Technology, Daejeon 34141, Korea*

²*Korea Research Institute of Standards and Science, Daejeon 34113, Korea*

*Corresponding Author address: kjchang@kaist.ac.kr

1. Calculation method

For Na-Si systems with various composition ratios, low-enthalpy allotropes were explored using an *ab initio* evolutionary crystal structure search method, as implemented in the AMADEUS code [1]. In this method, the conformational space annealing (CSA) algorithm [2] for global optimization is combined with first-principles electronic structure calculations. Since distinct configurations are generated, the CSA algorithm is very efficient to search for both stable and metastable configurations. The number of configurations was set to 30 in the population size of the CSA, and the enthalpy was used to express the objective function that describes specific target properties for a given pressure. For each configuration, the enthalpy was minimized by performing density functional theory calculations which employed the functional form of Perdew, Burke, and Ernzerhof (PBE) for the exchange-correlation potential [3] and the projector augmented wave potentials [4], as implemented in the VASP code [5]. The wave functions were expanded in plane waves up to an energy cutoff of 600 eV. For

Brillouin zone (BZ) integration, a k -point set was generated by a grid spacing of 0.15 \AA^{-1} . The ionic coordinates and lattice parameters were fully optimized until the residual forces and stress tensors were less than 0.02 eV/\AA and 1.5 kbar , respectively.

The phonon spectrum and EP coupling constant (λ) were obtained from first-principles density-functional perturbation theory as implemented in the QUANTUM ESPRESSO package [6]. The PBE exchange-correlation functional [3], ultrasoft pseudopotentials [7], and a plane wave basis set with an energy cutoff of 80 Ry were employed. The dynamical and electron-phonon interaction matrices were calculated using the $3 \times 3 \times 9$ and $9 \times 9 \times 9$ phonon-momentum grids for $P6/m\text{-Si}_6$ ($P6/m\text{-NaSi}_6$) and $sh\text{-Si}$, respectively. Then, denser $18 \times 18 \times 54$ and $54 \times 54 \times 54$ grids were adopted to perform the BZ integration in phonon-momentum space. The electron-phonon coupling $\lambda_{\mathbf{q}\nu}$ at a phonon wave vector \mathbf{q} for a phonon mode ν is related to the phonon linewidth $\gamma_{\mathbf{q}\nu}$, $\lambda_{\mathbf{q}\nu} = \gamma_{\mathbf{q}\nu}/2\pi\omega_{\mathbf{q}\nu}^2 N(0)$, where $\omega_{\mathbf{q}\nu}$ is the phonon frequency. The phonon modes contributed to the electron-phonon coupling can be analyzed from the Eliashberg function defined as, $\alpha^2 F(\omega) = \frac{1}{2} \sum_{\nu} \int_{\text{BZ}} \frac{d\mathbf{q}}{\Omega_{\text{BZ}}} \lambda_{\mathbf{q}\nu} \omega_{\mathbf{q}\nu} \delta(\omega - \omega_{\mathbf{q}\nu})$, where Ω_{BZ} is the BZ volume. Then, the frequency-dependent electron-phonon coupling is obtained from $\lambda(\omega) = 2 \int_0^\omega [\alpha^2 F(\omega')/\omega'] d\omega'$ and the electron-phonon coupling constant is given by $\lambda = \lambda(\infty)$.

2. X-ray diffraction pattern simulations

To guide the experimental identification of $P6/m\text{-NaSi}_6$, X-ray diffraction (XRD) patterns were simulated at 12.4 GPa [8]. The simulated XRD patterns of $P6/m\text{-NaSi}_6$ show a very strong peak around 40.49° , corresponding to the (121) diffraction, as shown in Fig. 3(a). The

other peaks (001), (101), (111), (201), and (211) correspond to $2\theta = 36.03^\circ$, 39.24° , 45.01° , 47.72° , and 55.24° , respectively. The lattice parameters of $P6/m\text{-NaSi}_6$ and its unit cell volume decrease after the Na removal. Therefore, the diffraction peaks of $P6/m\text{-Si}_6$ slightly shift to the higher 2θ values [Fig. 3(b)]. In $P6/m\text{-Si}_6$, additional peaks (100), (110), and (200) appear at $2\theta = 15.54^\circ$, 27.08° , and 31.37° , respectively.

3. Energy barriers for Na migration and stability identification

Figure 5(a) shows the migration pathway of a Na atom from site A to site B along the open channels in $P6/m\text{-NaSi}_6$ and $Cmcm\text{-NaSi}_6$. The migration barriers were calculated using the climbing image nudged elastic band (CI-NEB) method [9]. A $2\times 2\times 3$ supercell containing one Na and 72 host Si atoms was adopted. For $Cmcm\text{-NaSi}_6$ and $P6/m\text{-NaSi}_6$, the saddle points were found to be located within the Si layer between the A and B sites, and the energy barriers were calculated to be 0.65 and 0.48 eV per Na atom, respectively, using the PBE functional for the exchange-correlation potential [3] [Fig. 5(b)]. The lower energy barrier for Na migration in $P6/m\text{-NaSi}_6$ is because the large open channels are connected in a straight line to weaken the interaction between the guest and its surrounding Si atoms. Based on the results, it is expected that the Na degassing process can occur at lower temperatures in $P6/m\text{-NaSi}_6$ than $Cmcm\text{-NaSi}_6$. The dynamical stability of $P6/m\text{-NaSi}_6$ and $P6/m\text{-Si}_6$ at ambient pressure was verified by calculating the full phonon spectra (Fig. 4). In addition, the thermal stability of $P6/m\text{-NaSi}_6$ and $P6/m\text{-Si}_6$ at ambient pressure was examined by carrying out isothermal-isobaric molecular dynamics ($NpT\text{-MD}$) simulations up to 100 ps at 400 K [Figs. 2(b) and (c)]. To visualize the Na degassing process of $P6/m\text{-NaSi}_6$, we performed standard MD simulations at ambient pressure and 400 K for a slab geometry consisting of six Si layers and a vacuum

region of 8 Å, in which the (0001) surface is exposed to vacuum (see Fig. 6). At the same time, we found that the stability of the Si-based hexagonal lattice of NaSi₆ is maintained during the migration of Na along the open channels.

References

- [1] I.-H. Lee, Y. J. Oh, S. Kim, J. Lee, and K. J. Chang, Comp. Phys. Commun. **203**, 110 (2016).
- [2] J. Lee, I.-H. Lee, and J. Lee, Phys. Rev. Lett. **91**, 080201 (2003).
- [3] J. P. Perdew, K. Burke, and M. Ernzerhof, Phys. Rev. Lett. **77**, 3865 (1996).
- [4] P. E. Blöchl, Phys. Rev. B **50**, 17953 (1994).
- [5] G. Kresse and J. Furthmüller, Phys. Rev. B **54**, 11169 (1996).
- [6] P. Giannozzi, *et al.* J. Phys.: Condens. Matter **21**, 395502 (2009).
- [7] D. Vanderbilt, Phys. Rev. B **41**, 7892 (R) (1990).
- [8] I. Fujio and M. Koichi, Solid State Phenom. **130**, 15 (2007).
- [9] G. Henkelman, B. P. Uberuaga, and H. Jónsson, J. Chem. Phys. **113**, 9901 (2000).

TABLE 1. Crystal volumes (V in Å³ per Si-atom), densities of states at the Fermi level [$N(0)$ in states/Ry/Si-atom/spin], Electron phonon coupling constants (λ), logarithmic averages of phonon frequencies (ω_{\log} in K), and superconducting critical temperatures (T_c in K) for $P6/m$ -NaSi₆, $P6/m$ -Si₆, and simple hexagonal Si (*sh*-Si).

Allotrope	Pressure (GPa)	V	$N(0)$	λ	ω_{\log}	T_c
$P6/m$ -NaSi ₆	0	18.4	2.82	0.897	225	13.1
	15	16.1	2.60	0.498	331	4.0
$P6/m$ -Si ₆	0	16.8	2.40	0.799	263	12.2
	15	14.8	2.22	0.556	299	5.3
<i>sh</i> -Si	15	13.5	2.44	0.660	250	7.9

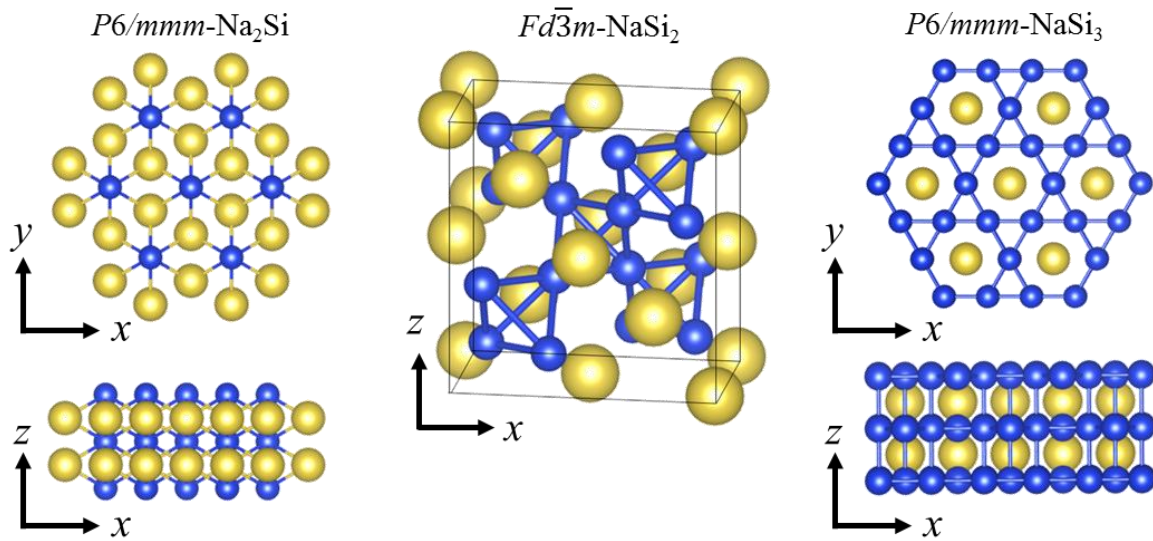


FIG. 1. Atomic structures of $P6/mmm$ -Na₂Si, $Fd\bar{3}m$ -NaSi₂, and $P6/mmm$ -NaSi₃ on the convex hull (Fig. 1 in the main manuscript). Blue and yellow spheres represent the Si and Na atoms, respectively.

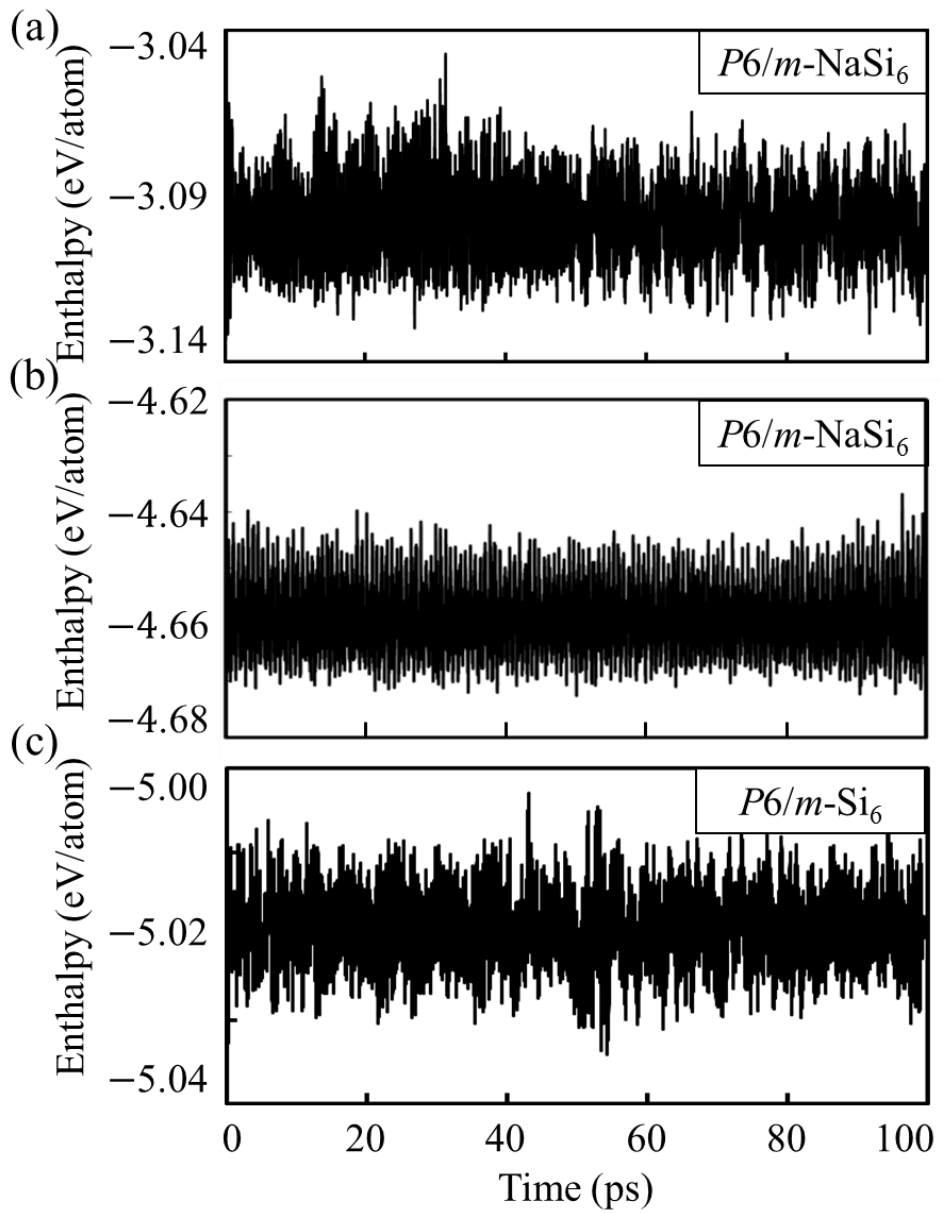


FIG. 2. Enthalpy fluctuations during NpT -MD simulations up to 100 ps for (a) $P6/m$ - NaSi_6 at 15 GPa and 1000 K, (b) $P6/m$ - NaSi_6 at zero pressure and 400 K, and (c) for $P6/m$ - Si_6 at zero pressure and 400 K. For both $P6/m$ - NaSi_6 and $P6/m$ - Si_6 , a $2 \times 2 \times 6$ supercell containing 144 host Si atoms is used.

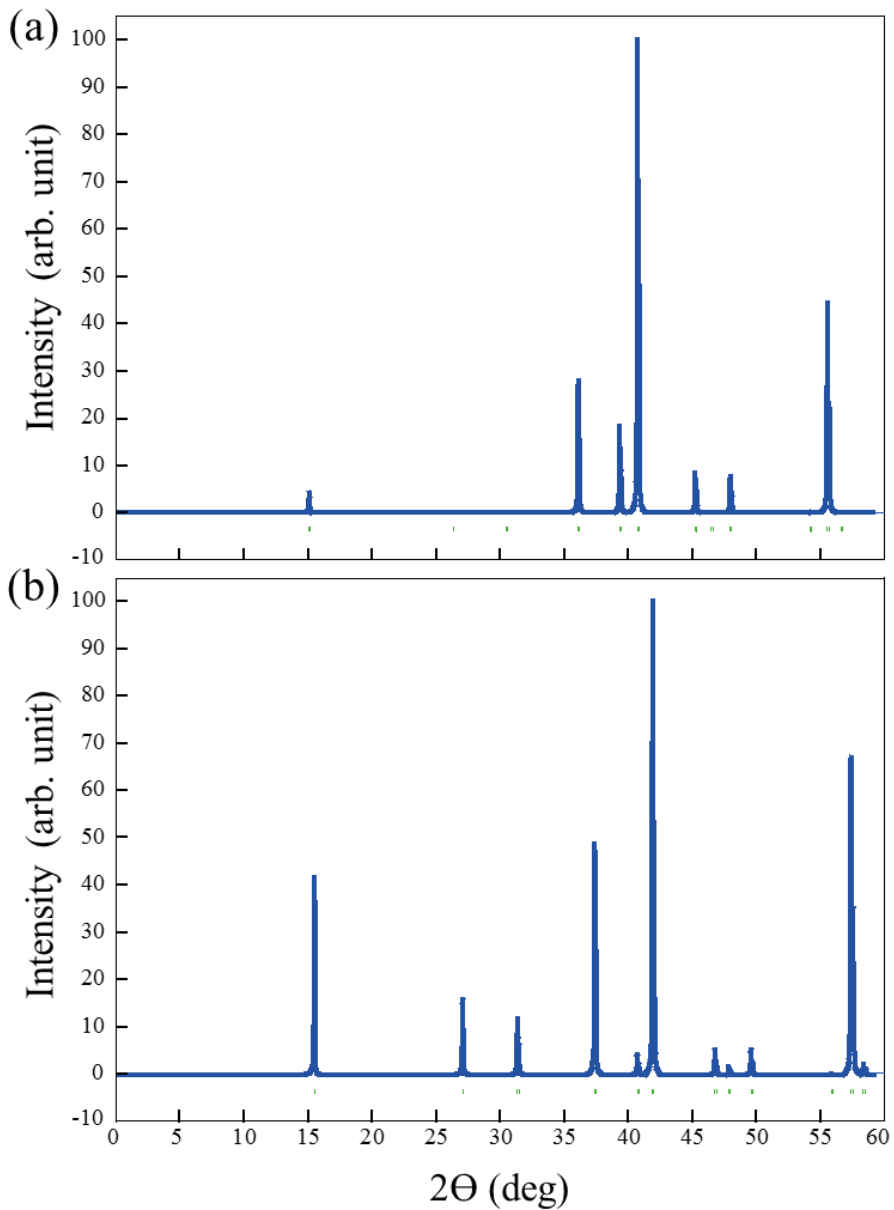


FIG. 3. The simulated X-ray diffraction patterns for (a) $P6/m\text{-NaSi}_6$ and (b) $P6/m\text{-Si}_6$ at 12.4 GPa. The lattice parameters of $P6/m\text{-NaSi}_6$ are $a = b = 6.762 \text{ \AA}$ and $c = 2.485 \text{ \AA}$, whereas those of $P6/m\text{-Si}_6$ are $a = b = 6.578 \text{ \AA}$ and $c = 2.403 \text{ \AA}$. A Cu source with the X-ray wavelength of 1.5406 \AA is assumed.

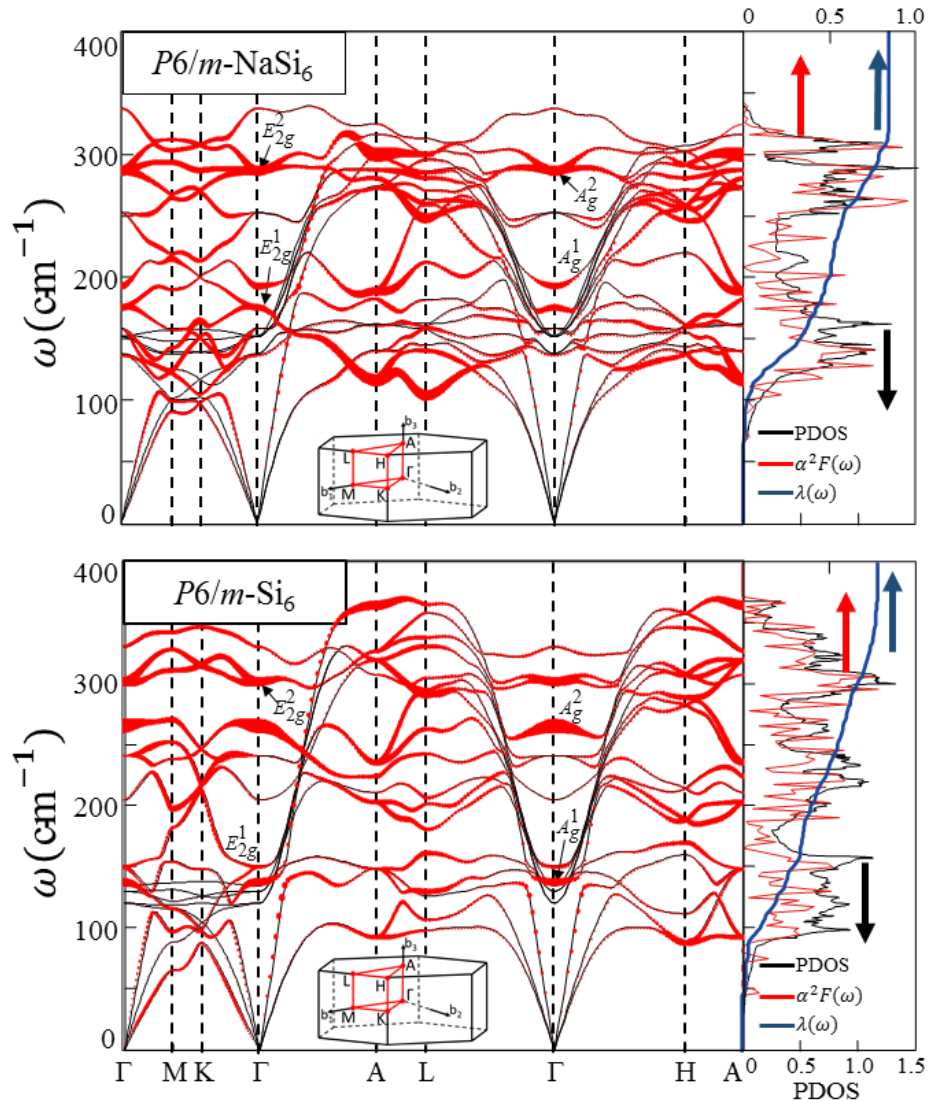


FIG. 4. The phonon spectra, phonon densities of states (PDOS in arb. unit), Eliashberg spectral functions $\alpha^2 F(\omega)$, and electron-phonon couplings $\lambda(\omega)$ for $P6/m\text{-NaSi}_6$ (top) and $P6/m\text{-Si}_6$ (bottom) at zero pressure. The magnitude of $\lambda(\omega)$ is indicated by the thickness of the red curves.

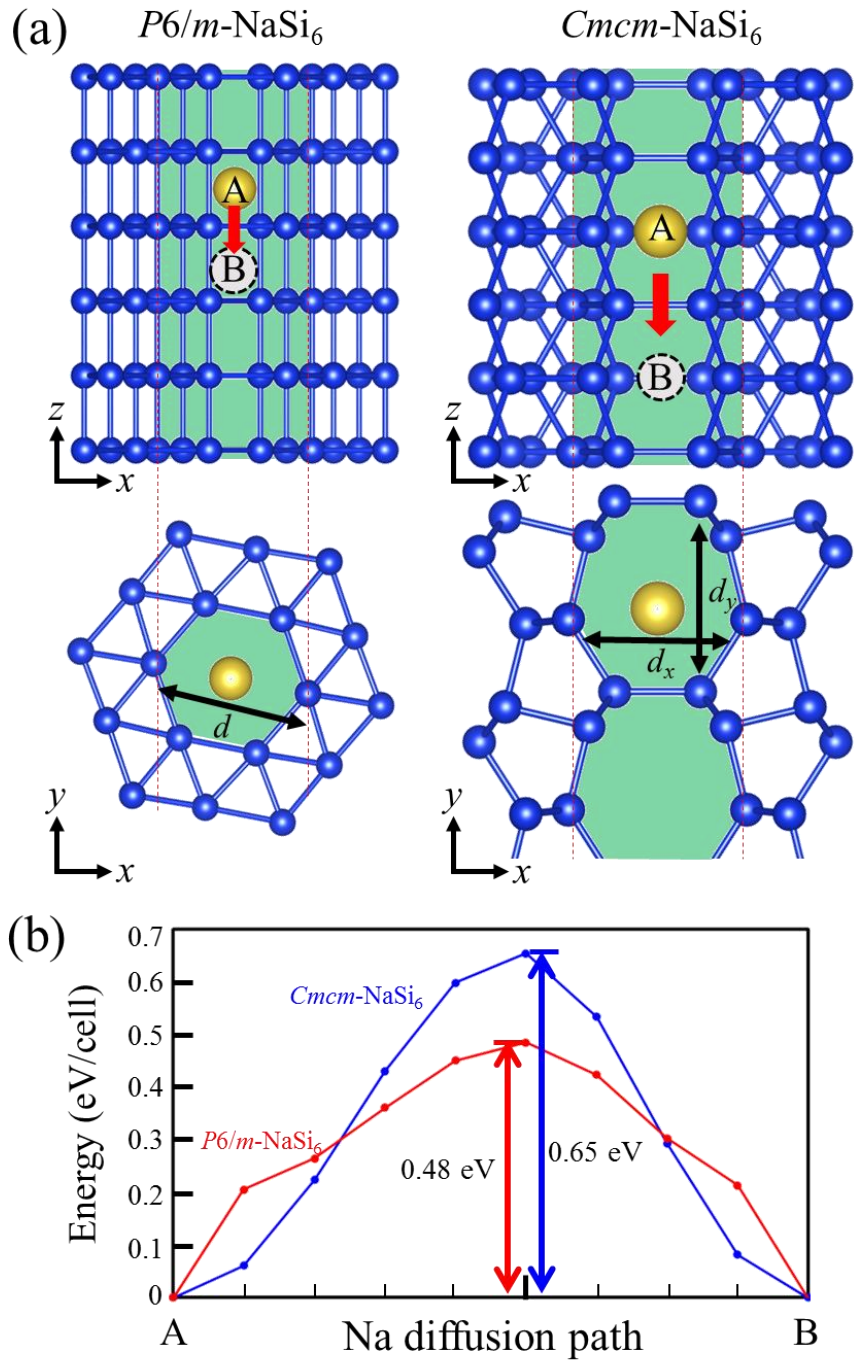


FIG. 5. (a) The migration pathways of the Na atoms along the open channels in *P6/m*-NaSi₆ and *Cmcm*-NaSi₆. The size of open channels is $d = 5.27 \text{ \AA}$ in *P6/m*-NaSi₆, and the channel sizes along the x and y directions are $d_x = 5.01 \text{ \AA}$ and $d_y = 5.29 \text{ \AA}$ in *Cmcm*-NaSi₆. (b) The energy barriers for Na migration along the open channels at zero pressure.

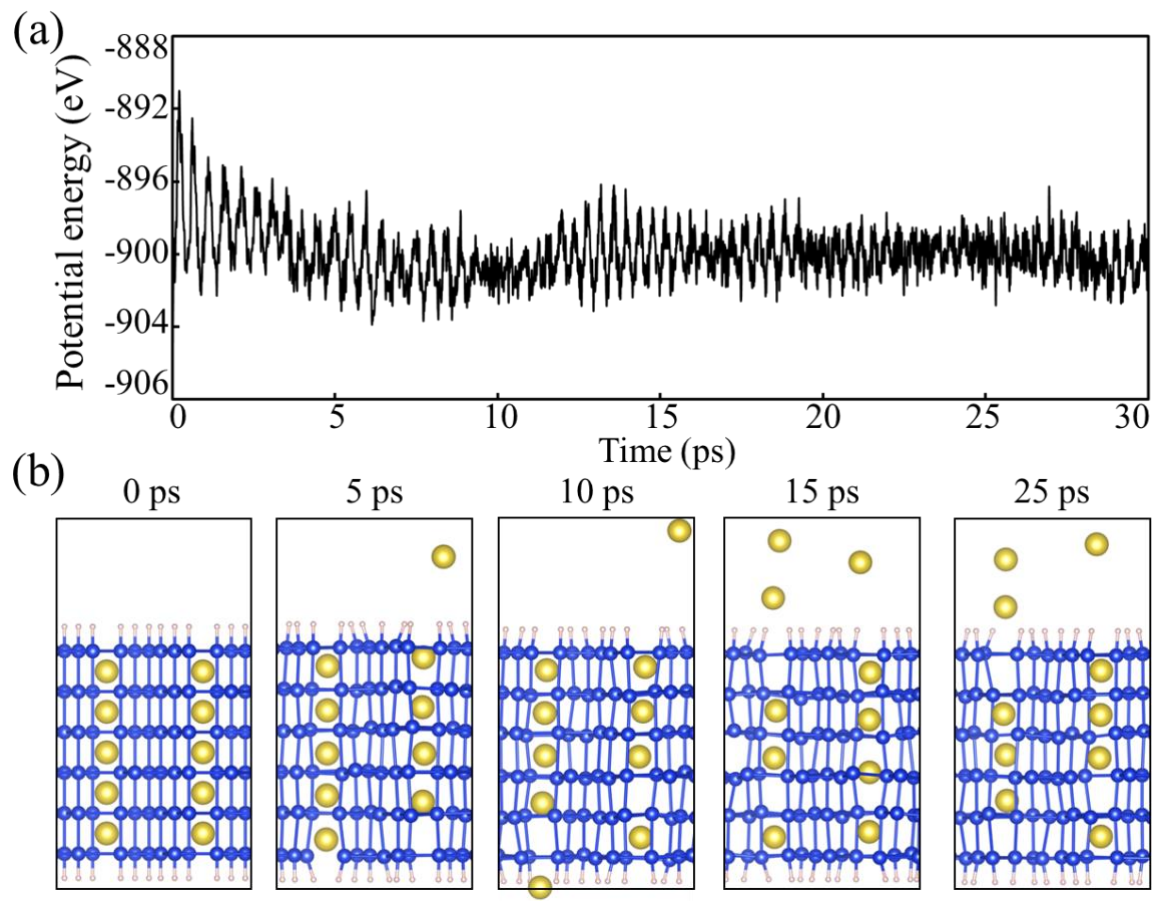


FIG. 6. (a) Potential energy fluctuations during standard MD simulations at zero pressure and 400 K for the degassing process using a slab geometry of $P6/m\text{-NaSi}_6$. (b) Side views of several selected configurations during MD simulations. Blue and yellow balls represent the Si and Na atoms, respectively.

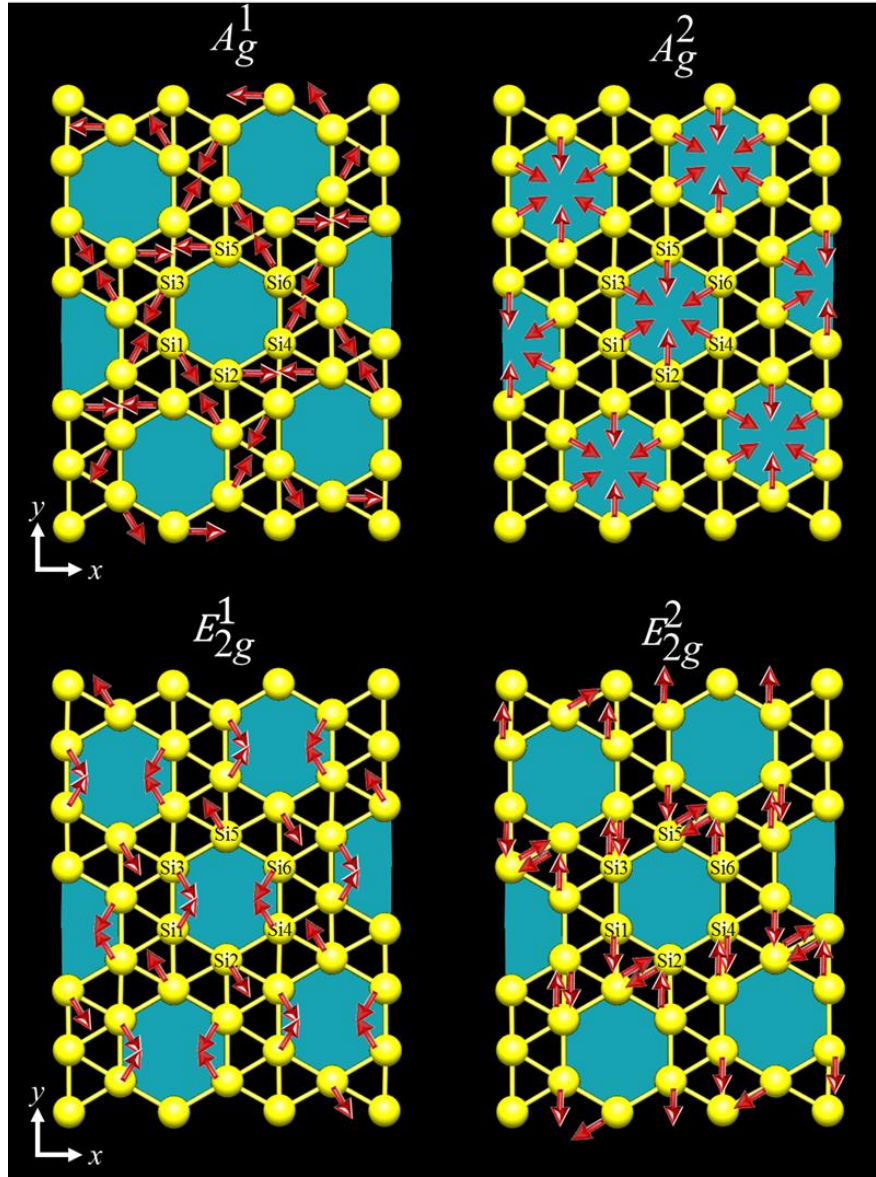


FIG. 7. Schematic illustrations of the atomic displacements of the Raman active A_g^1 , A_g^2 , E_{2g}^1 , and E_{2g}^2 modes at the Γ point in $P6/m$ -NaSi₆ and $P6/m$ -Si₆. Blue hexagons represent the open channels in top view. The A_g^1 and A_g^2 modes are associated with torsional and breathing motions of Si atoms around the open channels, respectively. The E_{2g}^1 and E_{2g}^2 modes are related to stretching and bending distortions of in-plane Si-Si bonds.

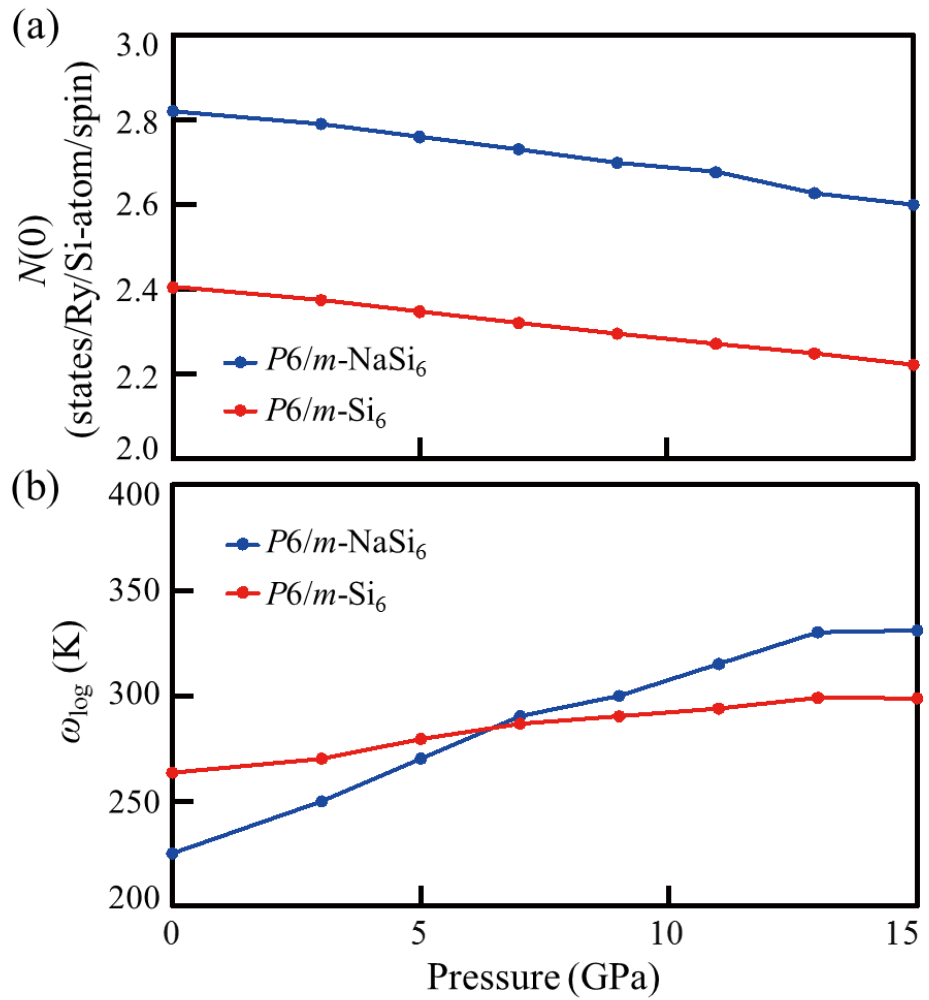


FIG. 8. (a) The electronic density of states at the Fermi level, $N(0)$, and (b) the logarithmic average of the phonon frequency, ω_{\log} , are plotted as a function of pressure for $P6/m\text{-NaSi}_6$ and $P6/m\text{-Si}_6$.